Fabrication of CVD graphene-based devices via laser ablation for wafer-scale characterization

Mackenzie, David; Buron, Jonas Christian Due; Whelan, Patrick Rebsdorf; Jessen, Bjarke Sørensen; Silajdi, Adnan; Pesquera, Amaia; Centeno, Alba; Zurutuza, Amaia; Bøggild, Peter; Petersen, Dirch Hjorth

Published in:
2D materials

Link to article, DOI:
10.1088/2053-1583/2/4/045003

Publication date:
2015

Document Version
Publisher's PDF, also known as Version of record

Fabrication of CVD graphene-based devices via laser ablation for wafer-scale characterization

2015 2D Mater. 2 045003

(http://iopscience.iop.org/2053-1583/2/4/045003)

2D Materials

RECEIVED
22 May 2015

REVISED
12 August 2015

ACCEPTED FOR PUBLICATION
7 September 2015

PUBLISHED
13 October 2015

PAPER

Fabrication of CVD graphene-based devices via laser ablation for wafer-scale characterization

David M A Mackenzie[1,2], Jonas D Buron[1,2], Patrick R Whelan[1,2], Bjarke S Jessen[1,2], Adnan Silajdźić[1,2], Amaia Pesquera[3], Alba Centeno[3], Amaia Zurutuza[3], Peter Bøggild[1,2] and Dirch H Petersen[1,2]

[1] Technical University of Denmark, Department of Micro- and Nanotechnology, Ørsteds Plads 345 B, Kgs. Lyngby, 2800, Denmark
[2] Center for Nanostructured Graphene (CNG), Technical University of Denmark, DK-2800 Kongens Lyngby, Denmark
[3] Graphenea S.A., Tolosa Hiribidea 76, E-20018 Donostia-San Sebastián, Spain

E-mail: dmac@nanotech.dtu.dk

Keywords: CVD graphene, laser cutting, wafer-scale graphene, picosecond laser, pulsed laser

Supplementary material for this article is available online

Abstract

Selective laser ablation of a wafer-scale graphene film is shown to provide flexible, high speed (1 wafer/hour) device fabrication while avoiding the degradation of electrical properties associated with traditional lithographic methods. Picosecond laser pulses with single pulse peak fluences of 140 mJ cm^{-2} for 1064 nm, 40 mJ cm^{-2} for 532 nm, and 30 mJ cm^{-2} for 355 nm are sufficient to ablate the graphene film, while the ablation onset for Si/SiO_2 (thicknesses 500 μm/302 nm) did not occur until 240 mJ cm^{-2}, 150 mJ cm^{-2}, and 135 mJ cm^{-2}, respectively, allowing all wavelengths to be used for graphene ablation without detectable substrate damage. Optical microscopy and Raman Spectroscopy were used to assess the ablation of graphene, while stylus profilometery indicated that the SiO_2 substrate was undamaged. CVD graphene devices were electrically characterized and showed comparable field-effect mobility, doping level, on–off ratio, and conductance minimum before and after laser ablation fabrication.

1. Introduction

While the introduction of copper-based catalytic chemical vapor deposition of graphene (Li *et al* 2010) has led to the scale-up to m^2-sized single layer graphene, the available methods for measuring the electrical properties of graphene are generally slow, inefficient and inadequate for large-area, large-volume characterization. The lack of large-area quality control can become an increasingly serious problem as the demand for throughput and consistency increases. The need of evaluating the homogeneity and quality of the graphene across such large areas is increasingly challenging. Standard lithographic methods are not only time-consuming, but unavoidably require graphene to come into contact with polymers/solvents/liquids that may permanently and adversely alter the electrical properties of graphene (Schedin *et al* 2007, Goossens *et al* 2012, Gammelgaard *et al* 2014). Such unintentional changes can be difficult to distinguish from sample-to-sample variations due to CVD growth and transfer parameters. As real applications emerge, the requirements with regards to quality and consistency are expected to increase further, and thereby making the need even greater for effective large-area quality management. Therefore a method which avoids traditional lithography would be an important improvement towards better large-scale characterization and device fabrication.

Previously it has been shown that femtosecond (Kalita *et al* 2011, Sahin *et al* 2014) and nanosecond (Kiisk *et al* 2013) pulsed lasers can ablate graphene. In this paper we expand on this previous work towards actual device fabrication and electrical characterization, and compare different wavelengths (355 nm, 532 nm and 1064 nm) of picosecond lasers to determine the optimal compromise between full laser ablation of graphene and avoidance of damage to the underlying SiO_2 substrate. We demonstrate that picosecond laser ablation is indeed a viable fabrication route for high-speed laser fabrication of wafer-scale graphene devices.

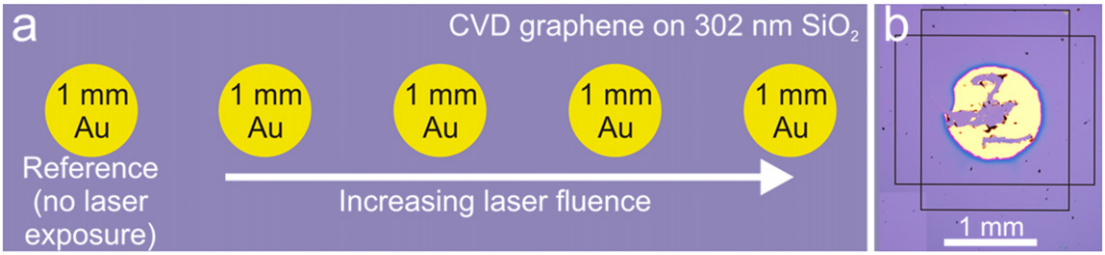

Figure 1. (a) Device layout for laser ablation tests. Testing is carried out by direct optical/Raman characterization and electrical measurements of conductance between individual electrodes and a reference electrode. (b) Optical image of Au electrode with laser ablation pattern of two overlapping rectangles with ablated lines colored in black for clarity.

2. Materials and methods

To investigate the ablation process of graphene films by intense 10 ps laser pulses, we utilize rows of circular 1 mm metal (Ti/Au 5/100 nm) electrodes with a 3.25 mm spacing (shown in figure 1(a)). These electrodes were deposited on monolayer CVD graphene by electron beam evaporation using a Wordentec QCL 800 system through a stencil shadow mask. CVD graphene covering a 4 inch Si wafer with 302 nm SiO_2 was supplied by Graphenea S.A. We exposed this graphene film to laser radiation of increasing fluence around each electrode to attempt to electrically isolate each Au electrode from the reference using a pattern of overlapping rectangles, as shown in figure 1(b). The single pulse fluence was increased for each device across the wafer. The single pulse fluence was in the range from a few to 400 mJ cm^{-2} with a writing time of less than 1 s per device and between 99 and 143 incident pulses per spot area. To detect the onset of graphene ablation we measured the electrical conductance between each electrode and a non-exposed reference Au electrode, and characterized the laser-exposed areas of graphene by micro-Raman spectroscopy and optical microscopy. Electrical characterization of graphene was performed using Keithley 2400 SMUs and a customized LabView program. The conductance between the reference electrode and each of the other electrodes was measured prior to laser writing with all conductance values falling in the 10^{-3} to 10^{-2} S range. Raman characterization was carried out using a Thermo Scientific DXR Raman Microscope at 445 nm wavelength using a 50x objective with each map containing 1600 spectra. In order to determine the position, intensity and width of Raman features of the graphene, individual Raman peaks were fitted in MatLab with a single Lorentzian function, as outlined in (Larsen *et al* 2014).

We investigated whether SiO_2/Si was unintentionally damaged by detecting recesses and protrusions using a Dektak XTA stylus profilometer with a 5 μm radius-of-curvature tip. Profilometer analysis was performed using a scan length of 120 μm, a scan time of 30 s, and a 13 nm per-pixel sampling with a stylus force of 3 mg.

Table 1. Laser writing parameters for picosecond lasers for the ablation of graphene.

Wavelength, λ	Radius, ω_0	Pulses per spot area
1064 nm	33.1 μm	99
532 nm	23.5 μm	141
355 nm	9.5 μm	143

Both laser cutting of aluminum stencil-masks and ablation of graphene was performed using a 3D-Micromac AG microSTRUCT vario laser micromachining system. The tool is equipped with picosecond lasers (pulse duration $\tau = 10$ ps) of 355 nm, 532 nm, and 1064 nm wavelengths, and a nanosecond laser ($\tau = 100$ ns) of wavelength 1064 nm. The nanosecond laser was used for the definition of a stencil mask in 400 μm thick aluminum. This system offers a laser spotsize of down to 19 μm diameter (FWHM), which enables accurate definition of millimeter-sized devices. The picosecond laser parameters used for the graphene ablation experiment are listed in table 1.

To avoid damage to the graphene device areas physical contact between the stencil mask and the graphene device areas was avoided during evaporation. This was achieved by ablating a 50 μm recess in the aluminum stencil mask around the areas where direct-mask contact would otherwise potentially touch the graphene. Prior to gold deposition, the stencil mask was annealed overnight under a 900 g aluminum block at 200 °C to reduce any warping induced during stencil manufacture.

3. Results and discussion

The optical microscope images of graphene devices for increasing laser fluence of the 532 nm laser in panels 2(a)–(d) show clearly distinguishable differences between undamaged graphene, electrically insulated graphene and areas where the substrate itself has been damaged. In order to confirm and characterize ablation and possible damage to the graphene, micro-Raman maps were produced in the regions where laser writing took place. Micro-Raman spectroscopy maps showing the 2D peak intensity of graphene below the

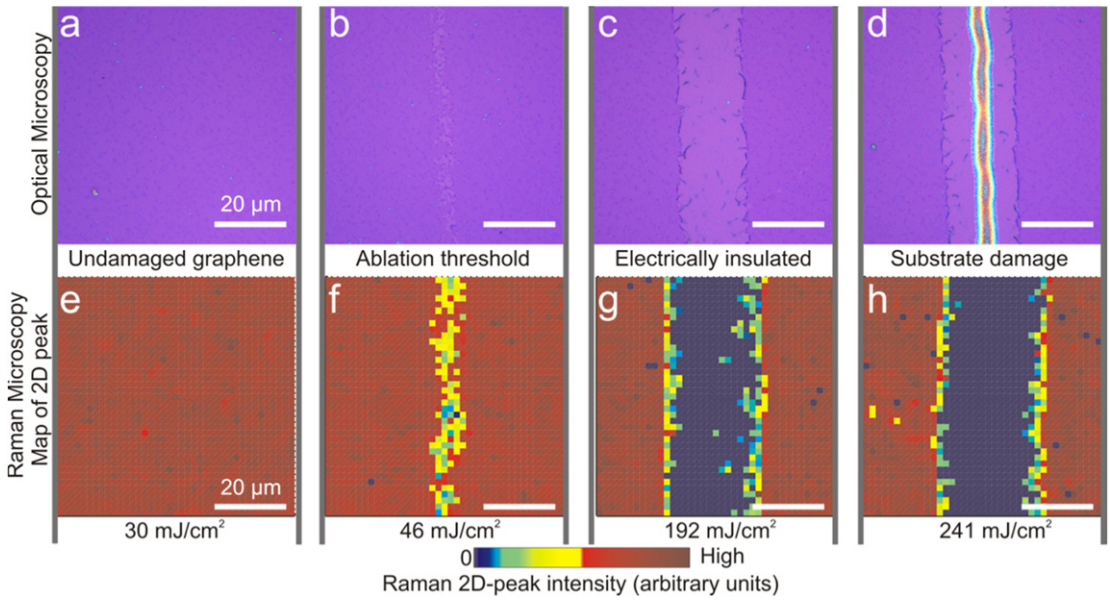

Figure 2. (a)–(d) Optical images showing onset of graphene ablation for 532 nm laser for increasing fluence. (e)–(h) Raman maps (2D-peak intensity) showing the onset of graphene ablation for 532 nm laser. Each Raman map incorporates 1600 spectra recorded over 3 s, with a 445 nm wavelength and a laser power of 5 mW.

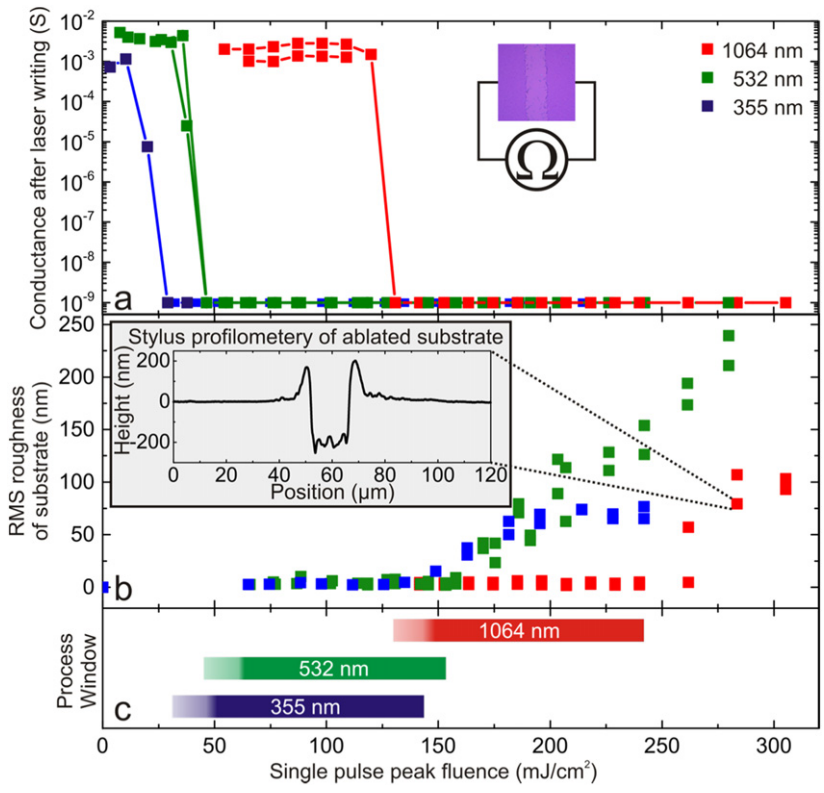

Figure 3. (a) Electrical characterization of picosecond laser ablated graphene. Conductance measurements as a function of single pulse fluence, obtained after laser writing with 1064 nm, 532 nm, and 355 nm wavelengths. (Inset) Example of height profile obtained with a stylus profilometer showing ablation of the substrate for the 1064 nm laser and a single pulse peak fluence of 284 mJ cm^{-2}. (b) Characterization of laser induced damage to SiO_2/Si substrate. rms value of height profile across laser ablation line as a function of single pulse fluence. (Inset) Example of height profile obtained with stylus profilometer. (c) Process windows for each laser wavelength with faded areas indicating electrical isolated fluences where rolled-up graphene remains on the surface.

graphene ablation threshold (panel (e)), at the transition towards graphene ablation (panel (f)), above the graphene ablation threshold (panel (g)), and above the SiO_2 ablation threshold (panel (h)). The absence of the 2D peak occurring above the graphene ablation threshold in figures 2(g) and (h), is an excellent

indicator of the absence of graphene (Ferrari and Basko 2013), and preferable compared to (2D peak intensity)/(G-peak intensity) ratio as normalization to the G-peak is pointless when there is no or poor graphene coverage. Areas where 2D peaks cannot be fitted in MatLab are set to zero in figures 2(e)–(h). The evolution of the (D-peak intensity)/(G-peak intensity) showed no increase in defect density in graphene below the ablation threshold. This data suggests that graphene exposed to a fluence below the ablation threshold is not being damaged.

The conductance between the reference electrode and each laser-exposed electrode are summarized in figure 3(a), which shows sharp transitions from a conducting state to an insulating state for all three wavelengths with a trend of smaller fluence for ablation onset with shorter laser wavelength. We also evaluated the damage to the underlying SiO_2 by stylus height profilometry, the results of which are shown in figure 3(b). Profilometer measurements showed no apparent substrate damage below a laser fluence of 240 mJ cm^{-2}, 150 mJ cm^{-2}, and 135 mJ cm^{-2} for 1032 nm, 532 nm and 355 nm, respectively, in figure 3(b). This is an important result as the ablation of oxide can deposit debris on the graphene areas of interest for electrical characterization, which means that issues with surface contamination can be avoided (Goossens *et al* 2012). Figure 3(c) shows the process window for each wavelength, defined as the single pulse peak fluence where graphene ablation occurs to the point where damage to the substrate is observed. For the three wavelengths, the process windows have a similar range, 105–115 mJ cm^{-2}. Other factors can be taken into consideration when choosing the optimal laser system for graphene device fabrication. For instance, the laser spotsize can be minimized to reduce the ablation linewidths. The laser-writing system used in this work was not optimized for minimal linewidth, and in the center part of the fabrication process window the linewidth was measured to be in the range 10–20 μm for all wavelengths. This is specific to the laser system and optics used, and is not a fundamental limit. The variation observed for different wavelengths in absorbed peak fluence required for graphene ablation will now be discussed.

The sharp onsets of graphene ablation (figure 3(a)), renders the graphene non-conducting at approximately 140 mJ cm^{-2} for $\lambda = 1064$ nm, 40 mJ cm^{-2} for $\lambda = 532$ nm, and 30 mJ cm^{-2} for $\lambda = 355$ nm. Although the intrinsic optical absorption of graphene across this wavelength range is constant at 2.3% (Nair *et al* 2008), interference effects in the 302 nm SiO_2 layer renders the effective optical absorption in the graphene layer wavelength dependent. In order to further investigate the wavelength dependence of the ablation process, a calculation was carried out for the graphene–SiO_2–Si stack (figure 4 inset) of the absorbed power in graphene as a function of wavelength. The fraction of power absorbed was calculated in the framework of the *transfer-matrix method* using the wavelength-dependent complex refractive indices for graphene (Weber *et al* 2010), SiO_2 (Gao *et al* 2013) and Si (Vuye *et al* 1993), with the angle of incidence assumed to be perpendicular to the sample. The absorption as a fraction of incoming power was calculated from the negative z-derivative of the Poynting vector. Most importantly, it was found that all significant absorption was in the graphene layer, and its magnitude is shown as a function of wavelength in figure 4(a). With the information gained from figure 4(a) we can present the absorption peak fluence in eV/atom, as shown in figure 4(b). The absorption peak fluence threshold for all wavelengths is now the same order (7 eV/atom) as (Wagman *et al* 1968, Shin *et al* 2014). The slightly broader value observed for 355 nm is attributed to measurement uncertainties in laser spotsize due to limited experimental resolution. However, because the onset of ablation appears to be below the C–C bond strength, we therefore propose a two-stage ablation mechanism that is consistent with our observations.

When graphene ablation occurs at lower laser fluences we propose a mechanism similar to the buckling explanation used to describe laser cleaning of surface films (Toth *et al* 1995, Luk'yanchuk 2002) which has previously been used to describe graphite ablation (Márton *et al* 1999). The buckling mechanism involves specific heating of the removed thin film (and not the substrate). For the case of graphene, our calculation above shows that the majority of the absorbed laser power occurs within the graphene layer. We can also infer, knowing the electron–phonon coupling time for graphene is a few picoseconds (George *et al* 2008, Sun *et al* 2008), that this energy is rapidly dissipated on the order of our laser-pulse length. The thermal expansion coefficient of graphene is known to be negative (Yoon *et al* 2011, De Andres et al 2012) and we speculate that this strain/contraction of graphene due to ps laser pulses could lead to rips/tears causing graphene to roll up on the surface. This is consistent with observations for lower fluences just above the graphene ablation threshold, shown in figure 4(c). Rolled-up graphene was only observed just above the onset of ablation. For most laser fluences in the process window a surface free from graphene was yielded, for example figure 4(d) which only shows rolled-up graphene at the ablation border. The lack of rolled-up graphene observed for higher fluences can be explained by the absorbed peak fluence per atom being above the C–C bond strength meaning that carbon atoms in these areas ablate simply via thermal breakage of bonds, followed by removal from the lattice. Whether such a combination of C–C thermal bond breaking and rolling-up of graphene induced at lower fluences can be independently confirmed or not, we recommend selecting a laser fluence above 7 eV/atom in order to obtain a substrate free from rolled-up graphene.

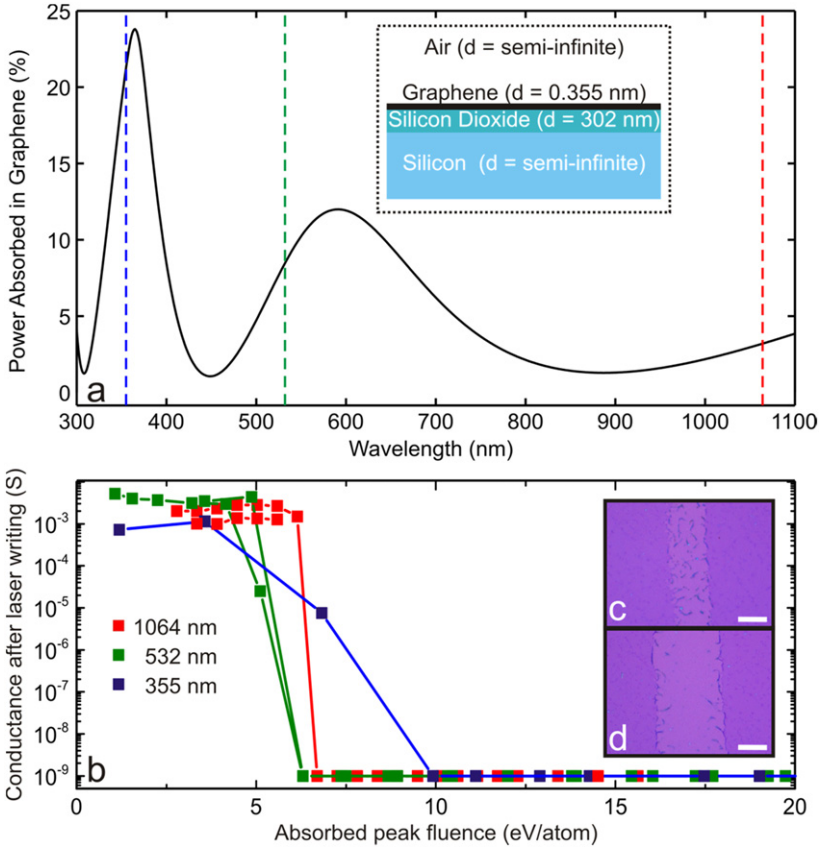

Figure 4. (Inset) Graphene–SiO_2–Si stack used in the framework of the transfer-matrix method to calculate: (a) Power absorbed in graphene for wavelengths in the range of 300–1100 nm. All significant absorption was in the graphene layer. Dashed lines represent the three wavelengths used in this paper. (b) Corrected version of figure 3(a), using the data from figure 4(a) which allows the absorbed peak fluence to be expressed in terms of eV/atom. (c) Optical microscopy image showing the rolling-up of graphene just above ablation threshold ($\lambda = 532$ nm, absorbed peak fluence $= 6$ eV/atom). (d) Optical microscopy image showing total graphene ablation with rolling-up only visible at edges ($\lambda = 532$ nm, absorbed peak fluence $= 8$ eV/atom). Scalebars are 10 μm.

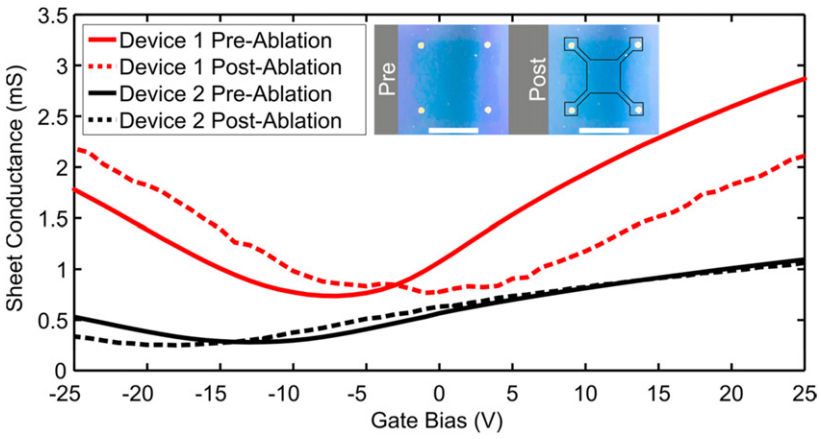

Figure 5. Electrical measurements of CVD graphene before laser ablation and after fabrication using the 1064 nm laser. (Inset) Close-up of single graphene device pre- and post-ablation with laser cuts false-colored in black for clarity. Scalebar is 5 mm. Additional electrical data is presented in the supplementary information.

Electrical measurements pre- and post-ablation were performed to evaluate if the laser ablation process affects the electrical properties of graphene. Van der Pauw devices were fabricated using the methods described above with the 1064 nm laser. An optical image of a typical device pre- and post-ablation is shown is inset of figure 5. Figure 5 shows examples of electrical measurements performed on CVD graphene, before and after laser ablation and are typical of the seven devices tested. We see that key electrical parameters such as conductance minimum, on–off ratio, and field-effect mobility are unaffected. For all

devices, the charge-neutrality point (CNP) shifts slightly up or down. Additional electrical data is presented in the supplementary information, as well as a comparison to a reference sample fabricated via electron beam lithography. We attribute the measured difference in CNP to variations within the graphene film rather than doping due to processing. This is somewhat expected when measuring a significantly smaller device area after ablation since the sample-to-sample variation in charge-neutrality-point position was higher than the pre/post ablation differences. The average position of the CNP showed a slight decrease after ablation over all devices, with device 1 exhibiting increased CNP as the only studied device. These results demonstrate that within the sample-to-sample variations, the graphene devices fabricated by laser ablation retained their electrical properties, and thus that this approach is a viable method for production of devices for the purpose of electrical characterization on the wafer-scale.

4. Conclusion and outlook

We show that using picosecond lasers of different wavelengths, graphene can be successfully ablated whilst causing no ablation of the silicon dioxide substrate. The processing windows of each of the wavelengths studied are of comparable size, and with absorbed peak fluence above 7 eV/atom recommended to obtain debris-free ablation. We showed that graphene absorbs the majority of absorbed power and we suggest a combination of two mechanisms for graphene ablation. At low fluences rips/tears are frequent, which results in graphene rolling up on the substrate and for higher peak laser fluences graphene ablation is caused by thermal breaking of C–C bonds. We suggest that this behavior is due to the localized heating and strain induced in graphene.

A 4 inch wafer with full graphene coverage can be turned into an array of individual devices with metal electrodes within an hour, and without damaging or affecting the properties of graphene, within our measurement uncertainty.

The advantages of the method compared to resist-based lithography methods include avoidance of contact with resist, solvents, water and the flexibility in matching the laser fluence to the substrate. This allows for a robust, fast, and accurate method for every-day characterization of the large-scale electrical properties of wafer-scale graphene. The method is thus well-suited for process optimization and quality assessment in relation to rapid prototyping as well as small- to medium scale production scenarios.

Acknowledgments

For funding we would like to acknowledge HC Ørsteds foundation, and Villum Fonden project no. VKR023117, and the DA-GATE project (12-131827) and EC Graphene FET Flagship contract number 604391. For help with the project we should like to acknowledge laser process specialists Chantal Silvestre and Peter Jesper Hanberg.

References

De Andres P L, Guinea F and Katsnelson M I 2012 Bending modes, anharmonic effects, and thermal expansion coefficient in single-layer and multilayer graphene *Phys. Rev.*B **86** 144103

Ferrari A C and Basko D M 2013 Raman spectroscopy as a versatile tool for studying the properties of graphene *Nat. Nanotechnology* **8** 235–46

Gao L, Lemarchand F and Lequime M 2013 Refractive index determination of SiO_2 layer in the UV/Vis/NIR range: spectrophotometric reverse engineering on single and bi-layer designs *J. Eur. Opt. Soc.—Rapid Pub.* **8** 13010

Gammelgaard L, Caridad J M, Cagliani A, Mackenzie D M A, Booth T J and Bøggild P 2014 *2D Mater.* **1** 035005

George P A, Strait J, Dawlaty J, Shivaraman S, Chandrashekhar M, Rana F and Spencer M G 2008 Ultrafast optical-pump terahertz-probe spectroscopy of the carrier relaxation and recombination dynamics in epitaxial graphene *Nano Lett.* **8** 4248–51

Goossens A M, Calado V E, Barreiro A, Watanabe K, Taniguchi T and Vandersypen L M K 2012 *Appl. Phys. Lett.* **100** 073110

Kalita G, Qi L, Namba Y, Wakita K and Umeno M 2011 *Mater. Lett.* **65** 1569–72

Kiisk V, Kahro T, Kozlova J, Matisen L and Alles H 2013 Nanosecond laser treatment of graphene *Appl. Surf. Sci.* **276** 133–7

Larsen M B B, Mackenzie D M, Caridad J M, Bøggild P and Booth T J 2014 Transfer induced compressive strain in graphene: evidence from Raman spectroscopic mapping *Microelectron. Eng.* **121** 113–7

Li X *et al* 2010 *Nano Lett.* **10** 4328–34

Luk'yanchuk B 2002 *Laser Cleaning* (Singapore: World Scientific) pp 328–39

Márton Z, Heszler P, Mechler Á, Hopp B, Kántor Z and Bor Z 1999 *Appl. Phys* .A **69** Supplement S133–6

Nair R R, Blake P, Grigorenko A N, Novoselov K S, Booth T J, Stauber T, Peres N M R and Geim A K 2008 *Science* **320** 1308

Sahin R, Simsek E and Akturk S 2014 Nanoscale patterning of graphene through femtosecond laser ablation *Appl. Phys. Lett.* **104** 053118

Schedin F, Geim A K, Morozov S V, Hill E W, Blake P, Katsnelson M I and Novoselov K S 2007 *Nat. Mater.* **6** 652–5

Shin H, Kang S, Koo J, Lee H, Kim J and Kwon Y 2014 Cohesion energetics of carbon allotropes: quantum Monte Carlo study *J. Chem. Phys.* **140** 114702

Sun D, Wu Z K, Divin C, Li X, Berger C, de Heer W A and Norris T B 2008 Ultrafast relaxation of excited Dirac fermions in epitaxial graphene using optical differential transmission spectroscopy *Phys. Rev. Lett.* **101** 157402

Vuye G, Fisson S, Nguyen Van V, Wang Y, Rivory J and Abelès F 1993 Temperature dependence of the dielectric function of silicon using *in situ* spectroscopic ellipsometry *Thin Solid Films* **233** 166–70

Toth Z, Hopp B, Kantor Z, Ignacz F, Szörényi T and Bor Z 1995 Dynamics of excimer laser ablation of thin tungsten films monitored by ultrafast photography *Appl. Phys.*A **60** 431–6

Wagman D D, Evans W H, Parker V B, Halow I, Bailey S M and Schumm R H 1968 *Selected Values of Chemical Thermodynamic Properties* National Bureau of Standards

Weber J W, Calado V E and van de Sanden M C M 2010 *Appl. Phys. Lett.* **97** 091904

Yoon D, Son Y W and Cheong H 2011 Negative thermal expansion coefficient of graphene measured by Raman spectroscopy *Nano Lett.* **11** 3227–31